A Novel Interferometric Sub-THz Doppler Radar With a Continuously Oscillating Reference Arm

Shaolin Liao, *Member, IEEE*, Nachappa Gopalsami, *Life Senior Member, IEEE*, Sasan Bakhtiari, *Senior Member, IEEE*, Thomas W. Elmer, II, Eugene R. Koehl, and A. C. Raptis

***Abstract*—In this paper, we have built and tested a mixerless sub-terahertz (sub-THz) Doppler radar consisting of just a continuous wave (CW) source and a Schottky diode intensity detector based on optical interferometry technique. The reference arm features an oscillating mirror to modulate the low-frequency-band (LFB) Doppler signature to the high-frequency-band (HFB) centered at the reference arm frequency. The reference arm frequency needs to oscillate at a frequency that is higher than twice the Doppler frequency of the object to avoid overlapping of the LFB and HFB signals. Rigorous mathematical formulas have been derived to solve for both the amplitude and the unambiguous phase of the Doppler signal, by using both LFB and HFB signals. The unwrapped phase can be obtained in two ways: a simply phase unwrapping process and a universal fitting process. The Doppler frequency signature of a moving object can be obtained from the Fourier transform of the phase. Computer simulation was first used to show the validity of the derived mathematical formulas. Then a prototype at 0.15 THz was built and tested using a ball pendulum as target. Experimental scenarios for phase span of less than 2π and greater than 2π were studied. The measured amplitude and phase have been shown to agree well with the set up experimental parameters.**

***Index Terms*—Continuous wave (CW), Doppler, interferometry, radar, sub-THz.**

I. Introduction

DOPPLER RADARS at microwave (MW) frequency [1]–[7] and millimeter-wave (mmW) frequency [8]–[13] have been extensively investigated in the past. At MW frequencies, Doppler radar is usually realized through the use of I-Q (quadrature) mixers. Doppler radar at mmW has also attracted a lot of attention in different applications [8]–[11]. Also recently, we have built and tested a 94-GHz Doppler radar based on I-Q mixer for remote monitoring of vital signs [12], [13]. Doppler radar at higher frequency (e.g., sub-THz and THz) calls for optical interferometry technique, due to either the lack of effective I-Q mixer at these frequencies or the simple implementation of interferometry architecture [14]–[17]. In our preliminary research in [18], we have built and tested a mixerless mmW (94 GHz) interferometric Doppler radar with a Continuous Wave (CW) source and a Schottky diode intensity detector only. Here we extend it to sub-THz range with a 0.15-THz prototype, taking into account of the background signal. The sub-THz Doppler radar employs a fast oscillating reference arm at a frequency greater than twice the maximum Doppler frequency. The detected intensity is the coherent addition of the reference beam and the reflected signal, which features a fast reference modulation on a slow modulation induced by the object. We have derived a rigorous mathematical formulation to solve for both the amplitude and the ambiguous unwrapped phase simultaneously, taking into account of the background scattering. Numerical simulation has been performed to confirm the validity of the mathematical formulas. We further built and tested a 0.15-THz prototype with a ball pendulum target of phase span of less than 2π and greater than 2π to study the performance of the interferometric sub-THz Doppler radar.

The paper is organized as follows. The principle and architecture of the interferometric sub-THz Doppler radar is presented in Section II, followed by the numerical simulation in Section III; experimental results in Section IV, discussion in Section V, and conclusions in Section VI.

Manuscript received November 07, 2013; revised January 20, 2014; accepted February 09, 2014. Date of publication March 11, 2014; date of current version April 29, 2014. This work is supported by the Office of Nonproliferation and Verification Research and Development under the National Nuclear Security Administration (NNSA) of Department of Energy under Contract DE-AC02-06CH11357.

The authors are with the Argonne National Laboratory, Argonne, IL 60439 USA (e-mail: sliao@ anl.gov).

Color versions of one or more of the figures in this paper are available online at http://ieeexplore.ieee.org.

Digital Object Identifier 10.1109/TTHZ.2014.2307165

II. Principle of the Interferometric Doppler Radar

A. Architecture of the Interferometric Doppler Radar

Fig. 1 shows the architecture of the studied sub-THz Doppler radar, which is based on the interferometry optics technique using a 0.15-THz CW source and a Schottky diode intensity detector. The source wave is first collimated into a parallel beam, which is then split into two beams, with one propagating towards the moving object and the other serving as the reference beam modulated by an oscillating mirror mounted on an oscillating motor driven by a power amplifier controlled by a function generator. The reflected Doppler signal by the moving object (blue beam in Fig. 1) is then combined with the reference beam (green beam in Fig. 1) and detected by the Schottky diode intensity detector.

B. Fundamental Principle

Mathematically, the intensity detector detects the combined reflected signal from the object $E_{\rm obj}(t)$ and the reference beam $E_{\rm ref}(t)$, plus the background E_b,

$$\begin{aligned} E(t) &= E_{\rm obj}(t) + E_{\rm ref}(t) + E_b \\ &= a_{\rm obj}(t)e^{j\phi_{\rm obj}(t)} + a_{\rm ref}e^{j\phi_{\rm ref}(t)} + a_b e^{j\phi_b} \end{aligned} \tag{1}$$

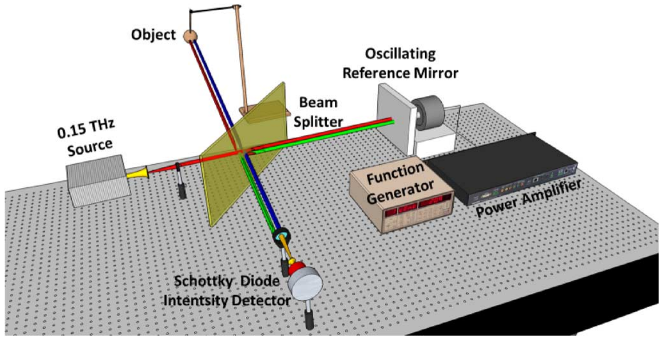

Fig. 1. Schematics of the proposed interferometric sub-THz Doppler radar architecture with just a CW source and an intensity detector.

where $a_{\rm obj}(t)$, $a_{\rm ref}$, and a_b are the amplitudes of the reflected signal, the reference beam and the background respectively; $\phi_{\rm obj}(t)$, $\phi_{\rm ref}(t)$ and ϕ_b are their corresponding phases. The detected intensity is thus given by

$$\begin{aligned} I(t) &= |E(t)|^2 \\ &= a_{\rm obj}^2(t) + a_{\rm ref}^2 + a_b^2 \\ &\quad + 2a_{\rm obj}(t)a_b\cos\left[\phi_{\rm obj}(t)-\phi_b\right] \\ &\quad + 2a_{\rm ref}a_b\cos\left[\phi_{\rm ref}(t)-\phi_b\right] \\ &\quad + 2a_{\rm ref}a_{\rm obj}(t)\cos\left[\phi_{\rm ref}(t)-\phi_{\rm obj}(t)\right] \end{aligned} \tag{2}$$

C. LFB and HFB Signals

The intensity signal given in (2) can be separated into LFB low-frequency-band (LFB) and high-frequency-band (HFB) signals. To illustrate this, let us decompose the reference phase $\phi_{\rm ref}(t)$ into Fourier series,

$$\phi_{\rm ref}(t) = \phi_0 + \sum_{m=1}^{\infty} c_m \cos(m\omega_{\rm ref}t). \tag{3}$$

Now let's consider the following term given in (2),

$$\begin{aligned} &2a_{\rm ref}a_b\cos\left[\phi_{\rm ref}(t)-\phi_b\right] \\ &= a_{\rm ref}a_b\left\{e^{j(\phi_{\rm ref}(t)-\phi_b)} + e^{-j(\phi_{\rm ref}(t)-\phi_b)}\right\} \\ &= a_{\rm ref}a_b\left\{e^{-j\widetilde{\phi}_b}e^{j\sum_{m=1}^{\infty}c_m\cos(m\omega_{\rm ref}t)}\right. \\ &\quad \left. + e^{j\widetilde{\phi}_b}e^{-j\sum_{m=1}^{\infty}c_m\cos(m\omega_{\rm ref}t)}\right\} \\ &= a_{\rm ref}a_b\left\{e^{-j\widetilde{\phi}_b}\prod_{m=1}^{\infty}\left[J_0(c_m)\right.\right. \\ &\quad \left. + 2\sum_{n=1}^{\infty}\left[j^nJ_n(c_m)\cos(nm\omega_{\rm ref}t)\right]\right] + e^{j\widetilde{\phi}_b}\prod_{m=1}^{\infty}\left[J_0(c_m)\right. \\ &\quad \left.\left. + 2\sum_{n=1}^{\infty}\left[(-j)^nJ_n(c_m)\cos(nm\omega_{\rm ref}t)\right]\right]\right\} \end{aligned} \tag{4}$$

where Jacobi–Anger expansion [19] has been used. J_0 is Bessel function of the first kind with order 0 and $\widetilde{\phi}_b = \phi_b - \phi_0$.

1) LFB Signal: The LFB signal from (4) is given by

$$2a_{\rm ref}a_b\cos\left[\phi_{\rm ref}(t)-\phi_b\right]\big|_{LFB} \approx 2a_{\rm ref}a_b\cos(\widetilde{\phi}_b)\prod_{m=1}^{\infty}J_0(c_m). \tag{5}$$

Similarly, the following term in (2) has a LFB signal of

$$\begin{aligned} &2a_{\rm ref}a_{\rm obj}(t)\cos\left[\phi_{\rm ref}(t)-\widetilde{\phi}_{\rm obj}(t)\right]\Big|_{LFB} \\ &\quad \approx 2a_{\rm ref}a_{\rm obj}(t)\cos\left(\widetilde{\phi}_{\rm obj}(t)\right)\prod_{m=1}^{\infty}J_0(c_m) \end{aligned} \tag{6}$$

where $\widetilde{\phi}_{\rm obj}(t) = \phi_{\rm obj}(t) - \phi_0$.

Hence the intensity given in (2) has the LFB signal of

$$\begin{aligned} &I(t)|_{LFB} \approx a_{\rm obj}^2(t) + a_{\rm ref}^2 + a_b^2 + 2a_{\rm obj}(t)a_b \\ &\cdot\cos\left[\widetilde{\phi}_{\rm obj}(t) - \widetilde{\phi}_b\right] \\ &+ 2a_{\rm ref}\prod_{m=1}^{\infty}J_0(c_m)\left\{a_b\cos(\widetilde{\phi}_b) + a_{\rm obj}(t)\cos\left(\widetilde{\phi}_{\rm obj}(t)\right)\right\}. \end{aligned} \tag{7}$$

2) HFB Signal: The amplitude of the HFB signal of the following term in (2) is given by

$$\begin{aligned} &2a_{\rm ref}a_b\cos\left[\phi_{\rm ref}(t)-\phi_b\right]\big|_{\rm HFB} \\ &\quad \approx 2a_{\rm ref}a_b\sin(\widetilde{\phi}_b)J_1(c_1)\prod_{m=2}^{\infty}J_0(c_m) \end{aligned} \tag{8}$$

Similarly, the following term in (2) has HFB signal amplitude of

$$\begin{aligned} &2a_{\rm ref}a_{\rm obj}(t)\cos\left[\phi_{\rm ref}(t)-\widetilde{\phi}_{\rm obj}(t)\right]\Big|_{HFB} \\ &\quad \approx 4a_{\rm ref}a_{\rm obj}(t)\sin\left(\widetilde{\phi}_{\rm obj}(t)\right)J_1(c_1)\prod_{m=2}^{\infty}J_0(c_m) \end{aligned} \tag{9}$$

Hence the intensity given in (2) has the HFB signal of

$$\begin{aligned} I(t)|_{HFB} &\approx 4a_{\rm ref}J_1(c_1)\prod_{m=2}^{\infty}J_0(c_m) \\ &\quad \times\left\{a_{\rm obj}(t)\sin\left(\widetilde{\phi}_{\rm obj}(t)\right) + a_b\sin(\widetilde{\phi}_b)\right\}. \end{aligned} \tag{10}$$

D. LFB and HFB Signals Without Background

The LFB and HFB signals without background interference [18] is obtained from (7) and (10)

$$\begin{aligned} I(t)|_{LFB} &\approx a_{\rm obj}^2(t) + a_{\rm ref}^2 \\ &\quad + 2a_{\rm ref}\prod_{m=1}^{\infty}J_0(c_m)a_{\rm obj}(t)\cos\left(\widetilde{\phi}_{\rm obj}(t)\right) \\ I(t)|_{HFB} &\approx 4a_{\rm ref}J_1(c_1)\prod_{m=2}^{\infty}J_0(c_m)a_{\rm obj}(t)\sin\left(\widetilde{\phi}_{\rm obj}(t)\right). \end{aligned} \tag{11}$$

E. Analytical Amplitude and Phase

The amplitude and phase of the object can be solved from the LFB signal in (7) and HFB signal in (10),

$$x_c(t)^2 + Bx_c(t) + C = I(t)|_{LFB} \tag{12}$$

where we have the following definitions:

$$\begin{aligned} x_c(t) &\equiv a_{\mathrm{obj}}(t)\cos\left(\tilde{\phi}_{\mathrm{obj}}(t)\right) \\ B &= 2a_b\cos(\tilde{\phi}_b) + 2a_{\mathrm{ref}}\prod_{m=1}^{\infty} J_0(c_m) \\ C &= x_s(t)^2 + a_{\mathrm{ref}}^2 + a_b^2 + 2a_b\sin(\tilde{\phi}_b)x_s(t) \\ &\quad + 2a_{\mathrm{ref}}a_b\cos(\tilde{\phi}_b)\prod_{m=1}^{\infty} J_0(c_m) - I(t)|_{LFB} \\ x_s(t) &\equiv a_{\mathrm{obj}}(t)\sin\left(\tilde{\phi}_{\mathrm{obj}}(t)\right) \\ &= \left[\frac{I(t)|_{HFB}}{4a_{\mathrm{ref}}J_1(c_1)}\prod_{m=2}^{\infty} J_0(c_m)\right] - a_b\sin(\tilde{\phi}_b). \end{aligned} \tag{13}$$

The variable $x_c(t)$ can be solved from (12),

$$x_c(t) = \frac{-B \pm \sqrt{B^2 - 4C}}{2}. \tag{14}$$

Combining (13) and (14), we obtain the amplitude and phase

$$a_{\mathrm{obj}}(t) = \sqrt{x_c(t)^2 + x_s(t)^2};\ \tilde{\phi}_{\mathrm{obj}}(t) = \arctan\left[\frac{x_s(t)}{x_c(t)}\right]. \tag{15}$$

F. Unwrapped Phase

We note that (15) only gives wrapped phase within $[0, 2\pi]$. There are two ways to do that: 1) phase unwrapping, i.e., we can obtain the unwrapped phase in (15) by using one-dimensional unwrapping algorithm and 2) fitting of (11), i.e., we can obtain the unwrapped phase directly by using fitting algorithm such as Levenberg–Marquardt algorithm [12] to fit both LFB and HFB signals in (11). The initial guess could be the wrapped phase obtained from (15) after some band-pass filter operation around the Doppler frequency to reduce the 2π phase jumps of the wrapped phase. Finally, a more universal way to solve (11) is to fit all experimental parameters and the unwrapped phase at the same time, which requires more sophisticated algorithm such as LM algorithm [12] and initial values.

G. Amplitude and Phase Without Background

When background is absent [18], the coefficients in (13) are given by

$$\begin{aligned} B &= 2a_{\mathrm{ref}}\prod_{m=1}^{\infty} J_0(c_m) \\ C &= x_s(t)^2 + a_{\mathrm{ref}}^2 - I(t)|_{LFB} \\ x_s(t) &\equiv a_{\mathrm{obj}}(t)\sin\left(\tilde{\phi}_{\mathrm{obj}}(t)\right) = \frac{I(t)|_{HFB}}{4a_{\mathrm{ref}}J_1(c_1)}\prod_{m=2}^{\infty} J_0(c_m). \end{aligned} \tag{16}$$

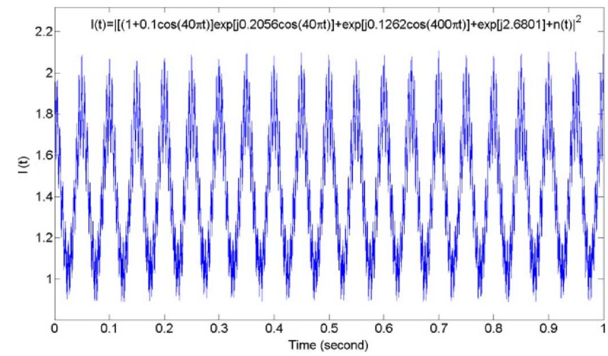

Fig. 2. Simulated intensity $I(t)$.

H. Doppler Signature

After we obtain the reflected sub-THz signal complex field (amplitude and phase), we can analyze the Doppler frequency signature of the moving object. The Doppler frequency $f_{\mathrm{Doppler}}(t)$ from the carrier frequency f is given by

$$f_{\mathrm{Doppler}}(t) = 2\frac{v(t)}{c}f \tag{17}$$

where $v(t)$ is the object velocity and c is the speed of light. The Doppler frequency is closely related to the phase $\phi_{\mathrm{obj}}(t)$ of the reflected signal for the object displacement $x(t)$,

$$f_{\mathrm{Doppler}}(t) = \frac{d\phi_{\mathrm{obj}}(t)}{dt} = \frac{4\pi}{\lambda}\frac{dx(t)}{dt} \tag{18}$$

where λ is the carrier wavelength. Equation (18) has taken into account the round trip of the carrier wave.

III. NUMERICAL SIMULATION

Before the experiment, we did some numerical simulation to confirm the mathematical derivation given in Section II. The following parameters are used for numerical simulation:

$$\begin{aligned} E(t) = [1 + 0.1\cos(40\pi t)]\,e^{j0.2056\cos(40\pi t)} \\ + e^{j0.1262\cos(400\pi t)} + e^{j2.6801} + n(t) \end{aligned} \tag{19}$$

where $n(t) = 0.1$ rand (t) is the added noise so that the SNR is 10 dB during the simulation. The intensity $I(t)$ plot is shown in Fig. 2. The calculated LFB and HFB signals are shown in Fig. 3. The reconstructed amplitude $a_{\mathrm{obj}}(t)$ and phase $\phi_{\mathrm{obj}}(t)$ are shown as red circles in Fig. 4, with very good agreements with the initial values (blue lines) in (19).

IV. EXPERIMENTAL RESULT

A. Experimental Description

To test the performance of the proposed interferometric Doppler radar, we built a 0.15-THz prototype using Gunn oscillator as a source and Schottky barrier (SB) diode as an intensity detector. The reference mirror is oscillating at a frequency of 190 Hz with amplitude of $A_{mirror} \approx 0.0388$ mm, much smaller than the wavelength of $\lambda = 2$ mm. This corresponds to the following parameters in (4): $c_1 = 4\pi A_{\mathrm{mirror}}/\lambda \approx 0.1218$,

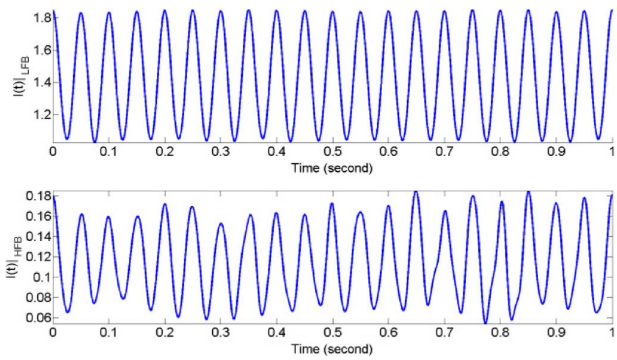

Fig. 3. LFB and HFB signals of $I(t)$ in Fig. 2.

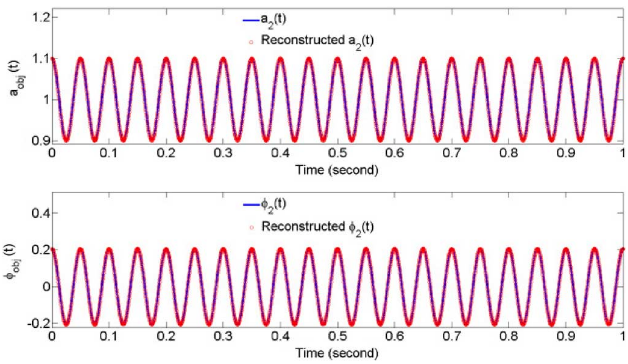

Fig. 4. Amplitude $a_{\rm obj}(t)$ and phase $\phi_{\rm obj}(t)$ obtained from LFB and HFB signals in Fig. 3: comparisons between reconstructed values and initial values in (19).

$J_1(c_1) \approx 0.0608$, $J_1(c_m) \approx 0$, $m = 2, 3, 4\ldots$; $c_m \approx 0$, $J_0(c_m) \approx 1$, $m = 1, 2, 3\ldots$. During the experiment, a swinging ball pendulum with length $L \approx 18$ cm is used as the Doppler object, giving a swing frequency [20] of $f_{\rm pendulum} \approx (1/2\pi)\sqrt{g/L} \approx 1.17$ Hz. The full swing distance of the swinging pendulum was set to a value much smaller than the carrier wavelength of $\lambda = 2$ mm.

B. Experimental Result and Analysis

Here we show results for two typical cases: 1) phase change smaller than 2π and 2) phase change larger than 2π.

1) Phase Change Smaller Than 2π: In this case, the full swing distance of the swinging pendulum was set to $D_{\rm pendulum} = 0.95$ mm. The measured intensity $I(t)$ has a SNR of ~8 dB, which is shown in the top plot of Fig. 5 and the zoom view of the first 0.5 s is shown in the bottom plot of Fig. 5, together with comparison with the theoretical fitting following (2). The LFB signal given in (7) and HFB signal given in (10) are shown in the top and bottom plots of Fig. 6, respectively.

With LFB and HFB signals obtained in Fig. 6, both amplitude and phase can be obtained by solving (12)to (14); Fig. 7 shows the obtained amplitude $a_{\rm obj}(t)$ and the phase $\phi_{\rm obj}(t)$ of the object. The full-swing phase, i.e., difference between the phase maximum $\phi_{\rm obj}(t)|_{\rm max}$ and the phase minimum $\phi_{\rm obj}(t)|_{\rm min}$, is obtained as $\approx 344^\circ$, which corresponds to a full-swing distance of $D_{\rm measured} \approx 0.96$ mm, agreeing well with the experimentally set value of $D_{\rm pendulum} = 0.95$ mm. Doppler frequency signature can be obtained through Fourier transform of $\phi_{\rm obj}(t)$ given in Fig. 8, which is shown in Fig. 7. The obtained pendulum frequency is $f_{\rm measured} \approx 1.21$ Hz, agreeing well with the aforementioned theoretical calculated value of $f_{\rm pendulum} \approx 1.17$ Hz.

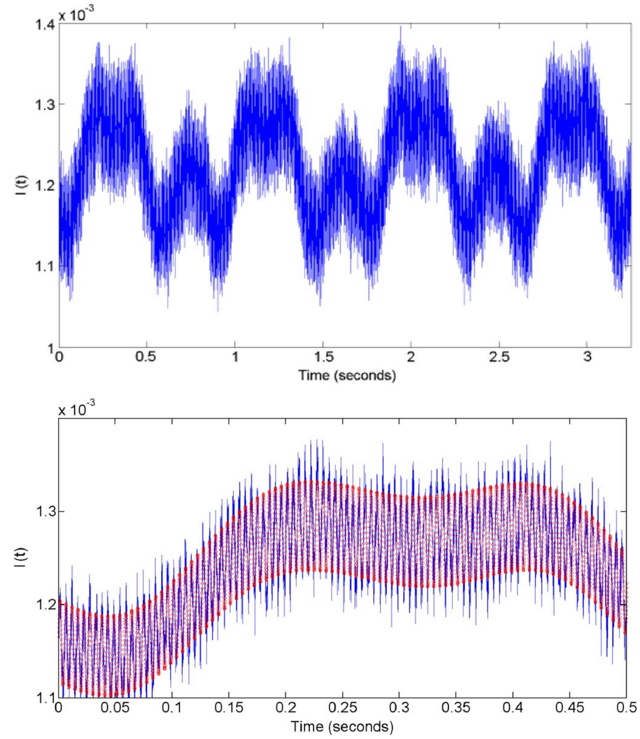

Fig. 5. (Top) measured intentisty $I(t)$ for a ball pendulum of small amplitude; and (bottom) zoom view of the first 0.5 second and the corresponding theoretical fitting (red circles).

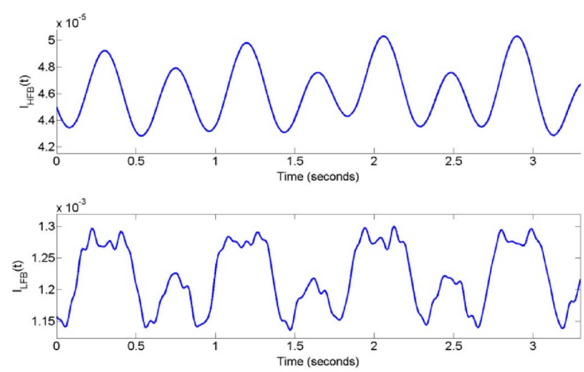

Fig. 6. (Top) HFB signal in (10); and (bottom) LFB signal in (7).

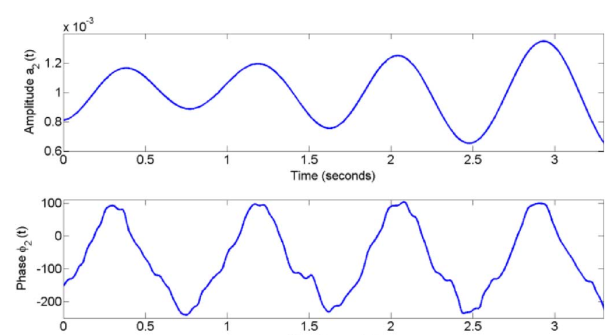

Fig. 7. (Top) amplitude $a_{\rm obj}(t)$; and (bottom) phase $\phi_{\rm obj}(t)$.

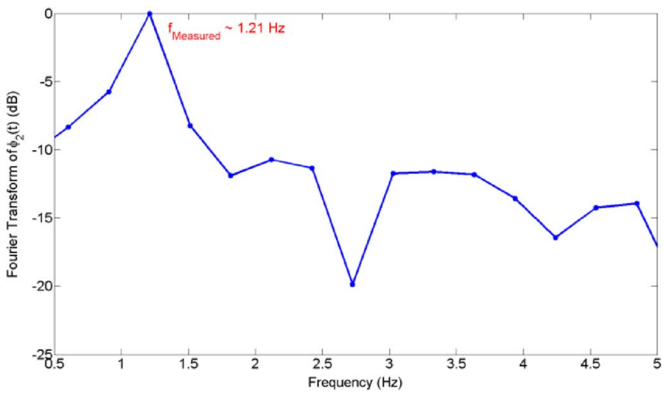

Fig. 8. Frequency signature obtained through Fourier transform of $\phi_{\rm obj}(t)$ given in Fig. 7.

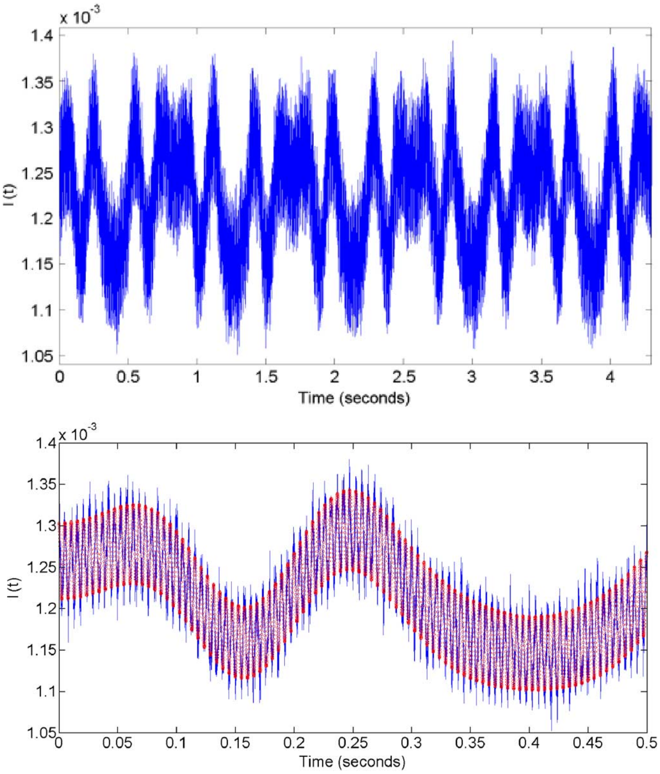

Fig. 9. (Top) measured intentisty $I(t)$ for a ball pendulum of large amplitude; and (bottom) zoom view of the first 0.5 second and the corresponding theoretical fitting (red circles).

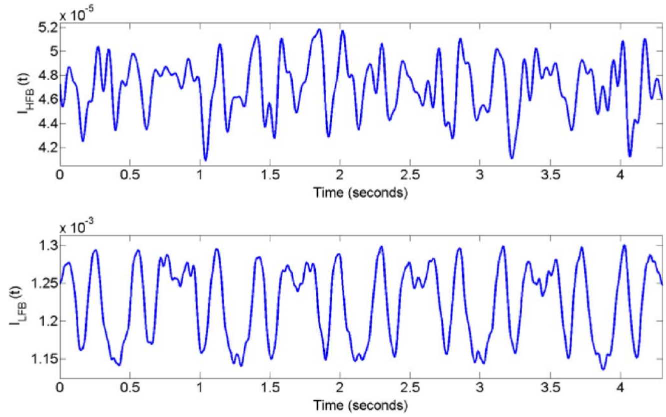

Fig. 10. (Top) HFB signal in Eq. (10), and (bottom) LFB signal in Eq. (7).

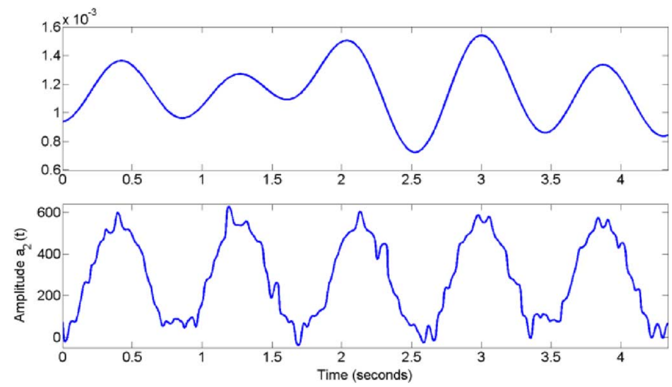

Fig. 11. (Top) amplitude $a_{\rm obj}(t)$, and (bottom) phase $\phi_{\rm obj}(t)$.

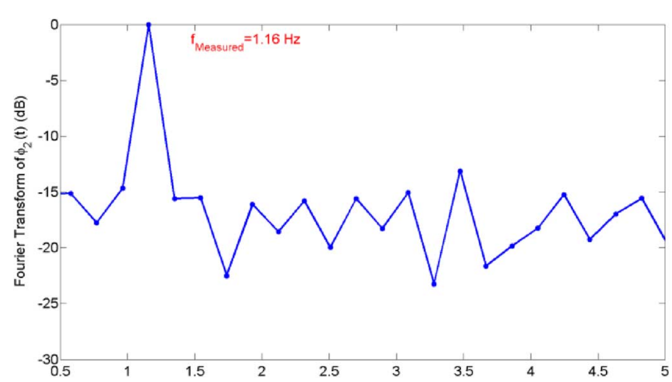

Fig. 12. Frequency signature obtained through Fourier transform of $\phi_{\rm obj}(t)$ given in Fig. 11.

2) Phase Change Larger Than 2π: In this case, the full swing distance of the swinging pendulum was set to $D_{\rm pendulum} = 1.85$ mm. The measured intensity $I(t)$ is shown in top plot of Fig. 9 and the zoom view of the first 0.5 s is shown in the bottom plot of Fig. 9, together with the theoretical fitting following (2). The LFB signal given in (7) and HFB signal given in (10) are shown in top and bottom plots of Fig. 10, respectively.

With LFB and HFB signals obtained in Fig. 10, both amplitude and unwrapped phase can be obtained by solving (12)to (14); Fig. 11 shows the obtained amplitude $a_{\rm obj}(t)$ and the phase $\phi_{\rm obj}(t)$ of the object. The full-swing phase, i.e., difference between phase maximum $\phi_{\rm obj}(t)|_{\rm max}$ and phase minimum $\phi_{\rm obj}(t)|_{\rm min}$, is obtained as $\approx 666^\circ$, which corresponds to a full-swing distance of $D_{\rm measured} \approx 1.8503$ mm, agreeing well with the experimentally set value of $D_{\rm pendulum} = 1.85$ mm. Doppler frequency signature can be obtained through Fourier transform of $\phi_{\rm obj}(t)$ given in Fig. 12, which is shown in Fig. 11. The obtained pendulum frequency is $f_{\rm measured} \approx 1.16$ Hz, compared with the theoretical calculated value of $f_{\rm pendulum} \approx 1.17$ Hz.

V. Discussion

We have shown that our novel interferometric Doppler architecture can obtain unwrapped phase in both less and greater than 2π scenarios by solving (11). There are two ways to unwrap the phase: 1) phase unwrapping followed by solving the analytical formulas in (15); and 2) a universal fitting process using sophisticated algorithms such as LM method to extract the experimental parameters and the unknown unwrapped phase. In both ways, we need to know the exact or approximate values of the experimental parameters such as $a_{\rm ref}$, and $c_{m=1,\ldots,\infty}$. In case 1), the accuracy of obtained unwrapped phase is very sensitive to these parameters. Fortunately, they can be carefully calibrated through standard procedure, e.g., using a known vibrating reference. In case 2) the initial values can vary somewhat within the convergence bound. Though better initial values make the algorithm converge faster. Finally, the $\mathrm{SNR} \sim 8$ dB can be improved by some band-pass filtering operation on the measured intensity, which is important for the analytical formula given by (15).

VI. Conclusion

We have successfully built and tested a mixer-less interferometric 0.15-THz Doppler radar. The sub-THz Doppler radar architecture consists of just a CW source and a Schottky diode intensity detector. A motorized oscillating reference mirror is used to modulate the intensity at a frequency higher than twice the object's Doppler frequency. We have derived a rigorous mathematical formulation to extract both the amplitude and the unambiguous phase of the Doppler signal by decomposing the measured intensity into LFB and HFB signals. The unwrapped phase can be obtained in two ways: phase unwrapping and parameters fitting. We first showed the validity of the mathematical analysis using computer simulation. Then a 0.15-THz prototype was built and tested using a ball pendulum for two scenarios: phase span less than 2π and greater than 2π.

References

[1] V. Lubecke, J. Li, and O. Boric-Lubecke, "A microwave radio for Doppler radar sensing of vital signs," in *2001 IEEE MTT-S Int. Microw. Symp. Dig.*, 2001, vol. 1, pp. 175–178.

[2] O. Boric-Lubecke, P. W. Ong, and V. M. Lubecke, "10 GHz Doppler sensing of respiration and heart movement," in *Proc. IEEE 28th Annu. Northeast Bioeng. Conf.*, Philadelphia, PA, USA, 2002, pp. 55–56.

[3] D. Obeid, S. Sadek, G. Zaharia, and G. El-Zein, "Non-contact heartbeat detection at 2.4, 5.8 and 60 GHz: A comparative study," *Microw. Opt. Technol. Lett.*, vol. 51, no. 3, pp. 666–669, 2009.

[4] D. Obeid, G. Zaharia, S. Sadek, and G. E. Zein, "Microwave Doppler radar for heartbeat detection vs. electrocardiogram," *Microw. Opt. Technol. Lett.*, vol. 54, no. 11, pp. 2610–2617, 2012.

[5] A. Thansandote, S. S. Stuchly, and A. M. Smith, "Monitoring variations of biological impedances using microwave Doppler radar," *Phys. Med. Biol.*, vol. 28, no. 8, pp. 983–990, 1983.

[6] M. Isa and Z. Wu, "Microwave Doppler radar sensor for solid flow measurements," in *Proc. 36th Eur. Microw. Conf.*, Manchester, U.K., 2006.

[7] P. Girao, E. Pinheiro, R. Madeira, J. M. D. Pereira, J. Mendes, G. Postolache, and C. Moura, "Multi-usage of microwave Doppler radar in pervasive healthcare systems for elderly," in *IEEE Instrum. Meas. Technol. Conf. (I2MTC)*, 2011, pp. 1–5.

[8] B. Geerts and Q. Miao, "The use of millimeter Doppler radar echoes to estimate vertical air velocities in the fair-weather convective boundary layer," *J. Atmosph. Oceanic Technol.*, vol. 22, 2005.

[9] H. Petersson, A. Nezirovic, M. B. Guldogan, and F. Gustafsson, "Millimeter-wave radar micro-Doppler signatures of human motion," in *2011 Proc. Int. Radar Symp. (IRS)*, 2011, pp. 167–174.

[10] E. M. Biebl, "A direction sensitive, integrated, low cost Doppler radar sensor for automotive applications," in *1998 IEEE MTT-S Int. Microw. Symp. Dig.* , 1998, vol. 2, pp. 1055–1058.

[11] M. C. Moulton, M. L. Bischoff, C. Benton, and D. T. Petkie, "Micro-Doppler radar signatures of human activity," in *Proc. SPIE 7837, Millim. Wave and THz Sensor and Technol. III*, 2010, vol. 78370L.

[12] S. Bakhtiari, S. Liao, T. W. Elmer, N. Gopalsami, and A. C. Raptis, "A real-time heart rate analysis for a remote millimeter wave I-Q sensor," *IEEE Trans. Biomed. Eng.*, vol. 58, no. , pp. 1839–1845, 2011.

[13] I. V. Mikhelson, S. Bakhtiari, T. W. Elmer, and A. V. Sahakian, "Remote sensing of heart rate and patterns of respiration on a stationary subject using 94-GHz millimeter-wave interferometry," *IEEE Trans. Biomed. Eng.*, vol. 58, no. 6, pp. 1671–1677, Jun. 2011.

[14] R. Meynart, "A simple interferometric vibrometer based on a laser Doppler velocimeter," *J. Phys. E: Scin. Instrum.*, vol. 17, 1984.

[15] A. A. Freschi, N. R. Caetano, G. A. Santarine, and R. Hessel, "Laser interferometric characterization of a vibrating speaker system," *Am. J. Phys.*, vol. 71, no. 11, pp. 1121–1126, 2003.

[16] T. Zure, J. Hernandez, and S. Chowdhury, "Dynamic analysis of an SOI based CMUT," in *IEEE Int. Conf. on Ind. Technol. (ICIT)*, 2012, pp. 539–544.

[17] Z. C. Bu, C. M. Zhang, and B. C. Zhao, "A static and divided mirror Michelson interferometer for measuring atmospheric winds," in *Proc. SPIE Int. Conf. on Optical Instrum. Technol.: Optical Syst. Optoelectron. Instruments*, 2008, vol. 7156, p. 71563D.

[18] S. Liao, N. Gopalsami, S. Bakhtiari, T. Elmer, and A. C. Raptis, "A novel interferometric mmW/THz Doppler radar," in *2013 IEEE Int. Instrum. Meas. Technol. Conf.*, Minneapolis, MN, May 6–9, 2013.

[19] M. Abramowitz and I. A. Stegun*, Handbook of Mathematical Functions With Formulas, Graphs and Mathematical Tables*. New York: Dover, ch. 9, p. 355.

[20] H. David, R. resnick, and J. Walker*, Fundamentals of Physics*, 5th ed. New York: Wiley, p. 381.

Shaolin Liao (GSM'07–M'13) received the B.S. degree in materials science and engineering from Tsinghua University, Beijing, China, in 2000, the M.S. degree in material science and M.S. degree in electrical and computer engineering, both from the University of Wisconsin at Madison, in August 2003 and December 2005, respectively and the Ph.D. degree in electrical and computer engineering from the University of Wisconsin at Madison, USA, in 2008.

He held the research fellow position in Physics Department, Queens College, City University of New York, from May 2008 to January 2010. He is currently with Argonne National Laboratory, Argonne, IL, USA. He has been interested in electromagnetics and its applications, which include, but not limited to, active and passive millimeter-wave applications like remote sensing, Non-Destructive Examination (NDE) and national security, both experiment and theory; high-power microwave transmission and conversion; gyrotron component design; microwave beam shaping technique; theory and algorithm development for high-performance simulation of electromagnetic wave propagation and scattering; antenna design and simulation. He has published more than 40 peer-reviewed papers and has three pending patents with Argonne National Laboratory.

Dr. Liao is a member of SPIE.

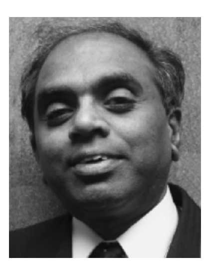

Nachappa (Sami) Gopalsami (S'77–M'79–SM'95–LSM'14) received the B.E. and M.S. degrees in electrical engineering from the University of Madras, India, and the Ph.D. degree in electrical engineering and computer science from the University of Illinois, Chicago, IL, USA.

He joined Argonne National Laboratory, Argonne, IL, USA, in 1980, where he is currently a Senior Electrical Engineer in the Sensors and Instrumentation section of the Nuclear Engineering Division. His current research interests include development of radio frequency, microwave, millimeter-wave, and terahertz sensors and imaging systems for national security, biosensing, environmental monitoring, and materials applications. He has published over 150 technical papers in the area of sensors and NDE and has five U.S. patents to his credit.

Dr. Gopalsami has received two R&D 100 awards from the R&D Magazine, both on millimeter wave sensors in 1986 and 2007; an outstanding paper award from the American Society of Nondestructive Testing; and an Outstanding Mentor award from the Office of Science Undergraduate Research Programs. He is a member of Sigma Xi and SPIE.

Sasan Bakhtiari (M'91–SM'94) received the B.S.E.E. degree from the Illinois Institute of Technology, Chicago, in 1983, the M.S.E.E. from the University of Kansas, Lawrence, KS, USA, in 1987, and the Ph.D. degree in electrical engineering from Colorado State University, Fort Collins, CO, USA, in 1992.

From 1984 to 1987, he was with the Radar Systems and Remote Sensing Laboratory, University of Kansas. From 1998 to 1992, he was with the Microwave Nondestructive Testing Laboratory, Colorado State University. In 1993, he joined Argonne National Laboratory, Argonne, IL, where he is currently an Electrical Engineer with the System Technologies and Diagnostics Department, Nuclear Engineering Division. He is also the Section Manager for the Nondestructive Evaluation (NDE) Section. He has authored or coauthored numerous technical publications in the areas of sensors and NDE.

Thomas W. Elmer, II received the B.S. degree in physics, with minors in mathematics and computer science, from La Sierra University in 1998, and the M.S. degree in physics from the University of Illinois, Chicago, IL, USA, in 2004.

While at La Sierra, he worked for the physics department, writing and maintaining programs to run laboratory experiments. He has also lectured on Astronomy and Gravitational Physics for the department. His senior research project was with the Health Physics department at Loma Linda University Medical Center, analyzing the activation of Cerrobend (R) metal by 250 MeV protons at the hospital's Proton Facility. In 1999, he joined Argonne National Laboratory, Argonne, IL, USA, as a student intern, eventually staying as a Software Engineering Associate for the System Technologies & Diagnostics Department of the Nuclear Engineering Division. He writes programming for modeling, motion control, data acquisition, and data analysis in the microwave, millimeter-wave, and terahertz sensors labs.

Mr. Elmers received an R&D 100 award from R&D Magazine in 2007.

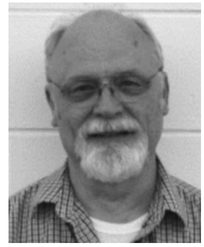

Eugene R. Koehl received the B.A. degree in physics from Lewis University, Romeoville, IL, USA, in 1969 and the B.S. degree in electrical engineering from Midwest College of Engineering (Illinois Institute of Technology), Chicago, IL, USA, in 1981.

He is an Electrical Engineer at Argonne National Laboratory, Argonne, IL, USA, with 37 years of experience in the design, fabrication, instrumentation, control, and automated data acquisition of experiments and facilities for testing the design and characteristics of sensors, power systems, and Liquid Metal Reactor (LMR) components. His activities cover a broad range of physical sciences, including acoustic signal transport, X-ray inspection and detection, high and process vacuum, alkali metal chemistry and heat transport, and satellite tracking and millimeter-wave systems. He has been involved with the precision manipulation and nondestructive testing of engineered materials used in heavy vehicle, stationary power, and aerospace systems for the past 16 years.

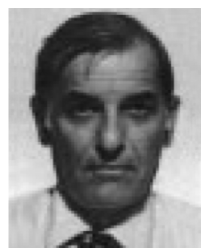

A. C. Raptis is a senior electrical engineer at Argonne National Laboratory, Argonne, IL, USA, with 35 years of experience in teaching and in research and development. His areas of expertise include sensors, instrumentation and controls, nondestructive evaluation, data processing, electromagnetics, plasmas, optics, acoustics and geophysical exploration. He is presently the department manager for Systems Technologies and Diagnostics in the Nuclear Engineering Division. At ANL he initiated and helped develop ANL's I&NDE (instrumentation and NDE) programs for nuclear and fossil energy, conservation and arms controls. These technologies include optics, microwaves/millimeter waves, acoustics, and neutron diffraction. He is responsible for work on national security for remote detection of chemical, biological, nuclear agents and explosives. In addition, he has been a strong participant in collaborative work with the University of Chicago in the development of the Bioengineering initiative. He is the author of more than 250 publications and holder of 17 patents.

Dr. Raptis is the recipient of the 1994, 1996, and 2007 R&D 100 awards, and 1994 ASNT best paper award.